Journal of Hazardous Materials 384 (2020) 121300

Contents lists available at ScienceDirect

Journal of Hazardous Materials

journal homepage: www.elsevier.com/locate/jhazmat

# Sono-electrodeposition of novel bismuth sulfide films on the stainless steel mesh: Photocatalytic reduction of Cr (VI)

Mahboobeh Zargazi[a], Mohammad H. Entezari[a,b,*]

[a] Sonochemical Research Center, Department of Chemistry, Faculty of Science, Ferdowsi University of Mashhad, Iran
[b] Environmental Chemistry Research Center, Department of Chemistry, Faculty of Science, Ferdowsi University of Mashhad, Mashhad, Iran

## GRAPHICAL ABSTRACT

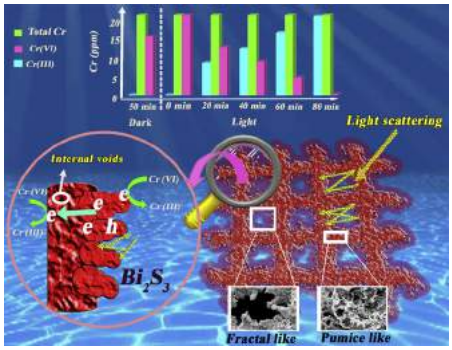


## ARTICLE INFO

Editor: Danmeng Shuai

*Keywords:*
Photocatalytic reduction
Cr (VI)
$Bi_2S_3$ film
Sono-electrodeposition
Pulse mode

## ABSTRACT

In this work, for the first time, bismuth sulfide ($Bi_2S_3$) film formed on the stainless steel mesh surface as a suitable substrate. Different films were synthesized by various combinations of the two methods (sonochemistry and electrochemistry) in continuous and pulse modes. The $Bi_2S_3$ films characterized by X-ray Diffraction (XRD), Scanning Electron Microscopy (SEM), Energy Dispersive X-ray Spectroscopy (EDS) and Atomic Force Microscope (AFM). To reach the best film for photocatalytic reduction of Cr (VI), different films were deposited on the substrate by changing three independent variables including pulse times ($t_{on}$, $t_{off}$) and sonication amplitude. Response Surface Methodology (RSM) applied for optimization of independent variables by using Central Composite Design (CCD). Here, the films prepared by sono-electrodeposition in pulse modes led to high photocatalytic efficiency in comparison with other films. The results confirmed that ultrasound affected the morphology of film due to the production of cavitation, micro jets and acoustic streaming. On the other hand, ultrasound decreased double layer thickness and dissolved diffusion problems. Sono-electrodeposition in pulse modes produced films with pumice and fractal like structures. The high photocatalytic activity attributed to special morphologies that have key roles in separation of hole/electron pairs and light multi-scattering.

* Corresponding author at: Sonochemical Research Center, Environmental Chemistry Research Center, Department of Chemistry, Faculty of Science, Ferdowsi University of Mashhad, Mashhad, Iran.
*E-mail address:* entezari@um.ac.ir (M.H. Entezari).

https://doi.org/10.1016/j.jhazmat.2019.121300
Received 8 April 2019; Received in revised form 22 September 2019; Accepted 22 September 2019
Available online 24 September 2019
0304-3894/ 

## 1. Introduction

Hexavalent chromium (Cr (VI)) is a common metal contaminant in water, which has attracted great attention around the world owing to its high toxicity and carcinogenic activity for humans and other creatures in nature (Hansen et al., 2003; Holmes et al., 2008). Therefore, it is of great necessity to explore how to remove Cr (VI) effectively in wastewater. Nowadays, processes of adsorption and photocatalytic reduction of Cr (VI) have been drawn much attention due to their cost-effectiveness, high stability, and environmental safety without adding any other contaminants. Among the applied photocatalyst materials used for degradation of pollutants, Bi-compounds have drawn more attention to researchers in this field. In previous works (Xu et al., 2018; Wu et al., 2013; Zargazi and Entezari, 2019a, b), triplet Bi-compounds were applied for degradation of organic pollutants in both forms of powder and film. The powder and film forms of $Bi_2WO_6$ synthesized by ultrasound and electrophoretic deposition were used for simultaneously degradation of binary mixtures of (RhB/MB) and (4-NP/4-CP). Bismuth sulfide ($Bi_2S_3$) as an another Bi-compound that is a typical lamellar structured semiconductor with a bulk direct band gap of 1.3 eV reduced photo-catalytically $CO_2$ and Cr (VI) (Jin and He, 2017; Luo et al., 2017). $Bi_2S_3$ compound in powder form suspended in the solvent and re-collected for reuse is a difficult task. To overcome this problem, the synthesis of films has been attracted by researchers recently (Buzea et al., 2007; Otsuka et al., 2008). $Bi_2S_3$ thin films deposited chemically and electrochemically for solar cells have been extensively studied in recent years. They have a suitable band gap for conversion of solar energy into electrical energy (Gao et al., 2011; Li et al., 2016; Velanganni et al., 2018). Pulse electrodeposition (PED) has been discovered as a new method for coating of nanometals onto different surfaces or defect sites (Nasiri Vatan et al., 2014). With PED method, a high overvoltage (high current density) is used in the same fashion as classical electrodeposition (ED), but the driving potential is applied for short periods of time. During the relaxation period (i.e., $t_{off}$), metallic ions migrate from the bulk to the surface region where ion consumption is highest (i.e., high local current density) and finally led to uniform distribution of metallic coatings on the surface compared to potentiostatic or galvanostatic ED (Chandrasekar and Pushpavanam, 2008). As reviewed by Kloke et al (Kloke et al., 2011), PED has advantages over classical ED. Namely relatively high localized concentration of the dissolved species during the relaxation time could be attributed to a higher crystal growth and electroactive surface area (Song et al., 2008). Non-uniform overgrowth of films or coatings on the electrode surface is known as one of the basic problems in ED. Another technique used to synthesize metallic films is sonochemical electrodeposition (SED). SED combines conventional ED with ultrasound. Some nanoparticles (Sáez and Mason, 2009) including platinum (Taguchi et al., 2016), CdSe nanotubes (Shen et al., 2008) and conductive polymers such as polyaniline (Ganesan et al., 2008) have been synthesized via the SED method. The SED technique reduces diffusion limitations by acoustic cavitation and micro-jet effects at the surface by interfering with the nucleating metal structure. Destabilizing bubbles formed during the deposition process also provide some convective mixing of dissolved ions within the mass boundary layer (González-García et al., 2010). However, similar to PED, the SED method is hindered by diffusion problems and also caused lack of control over particle size. To date, no previous methods have combined PED and pulse sonodeposition (PS) using a bimodal pulsing strategy for deposition of films onto electrode surface. Furthermore, $Bi_2S_3$ films were usually fabricated from non-aqueous solvents such as DMSO (Georges et al., 2007; Jana et al., 2009). Here, the technique is developed and called pulse sono-pulse electrodeposition (PS-PED). When both methods are in the pulse position in On and Off periods simultaneously, it is shown by the symbol (‖) and when one of them is in On and another is in Off period simultaneously, it is shown by the symbol (⊥). In addition, the deposition of $Bi_2S_3$ film on the stainless steel mesh as substrate is done in an aqueous solution (green synthesis). Stainless steel mesh (SS mesh) was used due to low cost, high chemical and mechanical stability and high harvesting capacity of light. Different films were synthesized under various combinations of two methods (electrochemistry and sonochemistry). To demonstrate the effect of pulse mode, deposition time, and sonication amplitudes on film quality, response surface methodology (RSM) was used to obtain optimized films for high photocatalytic reduction efficiency of Cr (VI).

## 2. Experimental section

### 2.1. Materials

Bismuth nitrate pentahydrate (Bi $(NO_3)_3$. $5H_2O$), sodium thiosulfate ($Na_2S_2O_3$), ethylene diamine tetra acetic acid (EDTA) and dichromate potassium ($K_2Cr_2O_7$) were purchased from Merck company. All of the applied materials used without further purification.

### 2.2. Synthesis of $Bi_2S_3$ film

The process of electrodeposition of $Bi_2S_3$ film on the substrate with details was as follows: $Na_2S_2O_3$ was dissolved in a mixture of distilled water and nitric acid with 90/10 ratio to form a solution of 40 mM. The yellowish colloidal solution was kept at room temperature for 24 h. After that, the yellow sulfur particles precipitated on the bottom of the beaker. The top clear solution used as electrodeposition bath. In addition, $Bi(NO_3)_3.5H_2O$ (0.006 M) and EDTA (0.006 M) were dissolved into the top solution. The stainless steel mesh plate (SS mesh) and Pt were placed as cathode and anode in the solution, respectively and a Ag/AgCl electrode used as reference electrode. The $Bi_2S_3$ thin films coated on the SS mesh surface at a cathodic potential of -1.5 V under different conditions (see Table 1) by Electro Analyzer (SAMA 500-Iran). Sonodeposiotion process alone was not able to deposit a film on the substrate. Therefore, electrochemical synthesis was used as a basic process for the formation of $Bi_2S_3$ film. After deposition, the as-prepared $Bi_2S_3$/SS mesh samples were washed several times by absolute ethanol and dried in a vacuum oven (Sci-Finthech, Korea) at 150 $^0$C for 90 min. The detailed procedure of the film synthesis schematically shown in Fig. 1. In the sono-electrodeposition method, horn system (Branson, digital sonifier 450, 20 kHz) applied for sonication of the system.

### 2.3. Characterization of $Bi_2S_3$ films

The crystallinity and phase of $Bi_2S_3$ films were investigated by X-ray Diffraction (XRD, Explorer GNR Italia) employing Cu Kα radiation, λ = 1.5418 Å. The shapes and elemental analysis of films were characterized by Scanning Electron Microscopy (SEM, LEO, Germany) equipped by Energy Dispersive X-Ray (EDS, Inca-350, Oxford Instruments elemental analyses). The thickness and morphology of

**Table 1**
Various methods for the synthesis of $Bi_2S_3$ films.

| Method | Electrochemistry mode | | Sonochemistry mode | |
|---|---|---|---|---|
| | Potential(V) | $t_{on}/t_{off}$ (s/s) | Amplitude | $t_{on}/t_{off}$ (s/s) |
| ED | −1.5 | ….. | ….. | ….. |
| PED | −1.5 | 4/8 | ….. | ….. |
| SED | −1.5 | ….. | 30% | ….. |
| S-PED | −1.5 | 4/8 | 30% | ….. |
| PS-ED | −1.5 | ….. | 30% | 4/8 |
| PS-PED* | −1.5 | 4/8 | 30% | 4/8(off/on) |
| PS-PED ** | −1.5 | 4/8 | 30% | 4/8 |

* Electrochemistry and sonochemistry systems were oppositely set in an on and off positions.

** Electrochemistry and sonochemistry systems were simultaneously set in an on and off position.

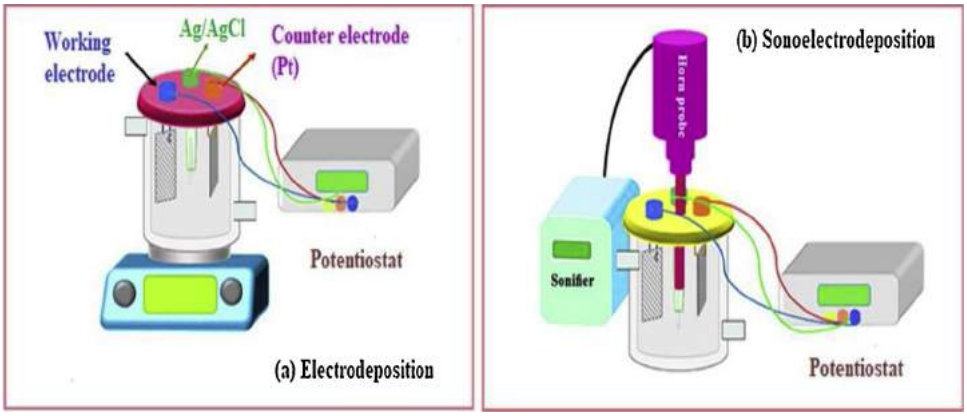


**Fig. 1.** Schematic representation of $Bi_2S_3$ film synthesis by (a) electrodeposition and (b) sono-electrodeposition methods.

films were investigated by Atomic Force Microscopy (AFM, Ara research, Iran). Optical microscopy (Olympus, SZH10) was also used to observe the appearance of films coated on the SS mesh.

### 2.4. Photocatalytic reduction activity of $Bi_2S_3$ film

The photocatalytic reduction of Cr (VI) was evaluated by the $Bi_2S_3$ films in a photocatalytic reactor described in our previous work (Zargazi and Entezari, 2019b, 2018). Cr (VI) solution was prepared from dissolved dichromate potassium ($K_2Cr_2O_7$) in distilled water. Cr (VI) solution with concentration of 22.5 ppm (20 mL) used for photocatalytic reduction studies. First, the film suspended in Cr (VI) solution and rotated with a specific speed in a dark place for obtaining adsorption-desorption equilibrium between film and pollutant solution. The photocatalytic reduction performance was evaluated via prepared film under direct sunlight radiation. For the best film of $Bi_2S_3$, the concentration of Cr(VI) ion and the total Cr were determined by recording the absorbance of sample solution at 350 nm using a UV–vis spectrophotometer (Unico 2008) and inductively coupled plasma atomic emission spectroscopy (ICP-AES, Spectro Arcos, Germany), respectively. The concentration of produced Cr (III) ions was measured by UV–vis and ICP-AES methods. To investigate the leaching and photocorrosion of $Bi_2S_3$ films, the concentration of Bi ion was evaluated by Flame Atomic Adsorption Spectroscopy (F-AAS, Nov AA 400 P, Germany) in dark and under photocatalytic process.

### 2.5. Response surface methodology (RSM)

The central composite design (CCD) was used to evaluate the influence of the independent parameters on the response function. The three independent parameters are $t_{on}$ ($X_1$), $t_{off}$ ($X_2$) and sonication amplitude ($X_3$). The levels of the three main selected variables are listed in Table 2. The expressions (−1), (0), and (+1), were used for low, medium, and high levels of the two-level-factorial design, respectively.

The independent factors coded according to the following equation (regression equation developed by Box-Hunter) (1).

**Table 2**
Independent variables and their levels.

| Symbol | Parameters | Coded levels | | |
|---|---|---|---|---|
| | | −1 | 0 | +1 |
| $X_1$ | $t_{on}$ (Sec) | 4 | 8 | 12 |
| $X_2$ | $t_{off}$ (Sec) | 4 | 8 | 12 |
| $X_3$ | Sonication amplitude (%) | 20 | 40 | 60 |

$$Xi = \frac{(Xi - X0)}{\Delta Xi} \quad (1)$$

where $X_i$ and $x_i$ are the dimensionless value and the real value of the independent parameter, respectively. $x_0$ and $\Delta x_i$ are also parameter values at the central point and the step change, respectively (Li et al., 2013). The relationship between predicted response and effective parameters is given by Eq. (2).

$$Y = \beta_0 + \Sigma_{i=1}^{k}\beta_i x_i + \Sigma_{i=1}^{k}\beta_{ii} x_i^2 + \Sigma_i \Sigma j\, \beta_{ij} x_i xj + \varepsilon \quad (2)$$

where Y is the predicted response, $\beta_0$, $\beta_i$ and βij are the offset term, linear, and squared influences, respectively. The interaction effect between two parameters also displayed by term $\beta_{ii}$. In addition, ε represents the error in statistical calculations. The analysis of variance (ANOVA) was selected to compare of the proposed model and examine results of the experimental design.

The CCD method designed 20 runs for three independent variables that shown in Table 3. The films obtained from designed experiments were applied for photocatalytic reduction of Cr (VI). The best reduction efficiency obtained at optimum time of 30 min. Therefore, the reduction efficiencies investigated were based on a fixed time of 30 min. Furthermore, the optimal values of the selected variables obtained using numerical optimization method provided by the Design-Expert 10

**Table 3**
Design of experiments and real responses.

| Run | $T_{on}$ (sec) | $T_{off}$ (sec) | Sonication amplitude (%) | Photocatalytic reduction (%) |
|---|---|---|---|---|
| 1 | 0 | 0 | +1 | 98.53 |
| 2 | −1 | +1 | +1 | 26.25 |
| 3 | 0 | 0 | 0 | 75.14 |
| 4 | 0 | −1 | 0 | 83.37 |
| 5 | +1 | −1 | +1 | 31.02 |
| 6 | −1 | 0 | 0 | 52.10 |
| 7 | −1 | −1 | −1 | 27.37 |
| 8 | 0 | 0 | 0 | 74.67 |
| 9 | 0 | 0 | −1 | 14.06 |
| 10 | 0 | +1 | 0 | 65.39 |
| 11 | 0 | 0 | −1 | 38.23 |
| 12 | −1 | +1 | −1 | 41.02 |
| 13 | 0 | 0 | 0 | 75.17 |
| 14 | +1 | 0 | 0 | 19.30 |
| 15 | −1 | +1 | +1 | 26.05 |
| 16 | 0 | 0 | 0 | 75.09 |
| 17 | 0 | −1 | 0 | 83.51 |
| 18 | +1 | −1 | +1 | 31.38 |
| 19 | 0 | 0 | 0 | 75.13 |
| 20 | 0 | 0 | 0 | 75.21 |

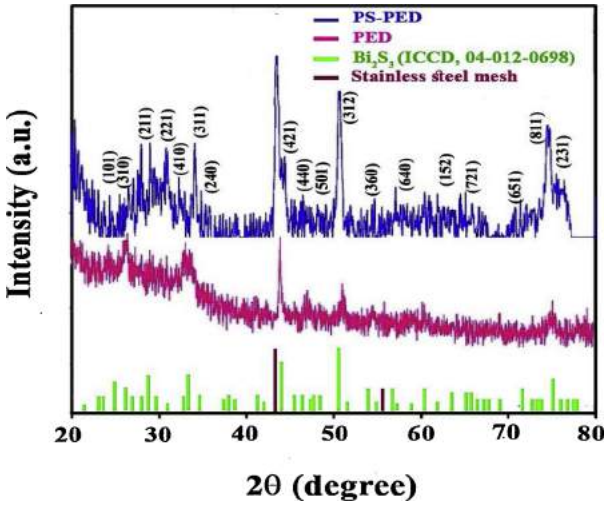


**Fig. 2.** XRD patterns of films synthesized by PED and PS-PED methods.

software.

## 3. Results and discussions

### 3.1. Characterization of $Bi_2S_3$ films

Fig. 2 presents the XRD patterns of $Bi_2S_3$ films that were synthesized by two the methods of PED and PS-PED (‖). All diffraction peaks were attributed to orthorhombic phase of Bi2S3 (ICCD, No: 04-012-0698) without impurity. Film synthesized by PED method demonstrated lower intensity of peaks in comparison with the film obtained by PS-PED method. This means that the presence of ultrasound led to more growth of crystallography plates of $Bi_2S_3$ compound.

Appearance of films were shown in images, Fig. 3 (a and d), taken by optical microscopy. It shows that the PS-PED method led to a higher dense and porous film with light red color compared to the PED method. The shapes of the deposited layers presented by SEM images are shown in Fig. 3. The images in Fig. 3(b, c) demonstrated the growth of film prepared by PS-PED method and Fig. 3 (e, f) presented the films synthesized by PED method. The fractal like structures between the wires at SS mesh are shown in Fig. 3c. This structure can be attributed to the presence of ultrasound during the electrodeposition. Ultrasound produces cavitation, shock waves and acoustic streaming in solutions and leads to reduce the dendrite-like structures, enhance the reach of ions to electrical double layer, and produce more nucleation sites for the growth step. But in the case of PED method, during the relaxation time ($t_{off}$), the dendrite like structures can be dissolved and overcome the diffusion problem of ions to the surface electrode. This mechanism caused the formation of layered structures of films that is clearly observed in Fig. 4a. In PS-PED method, the sonication and electrodeposition are in pulse modes and both of them are simultaneously in On and Off positions. These conditions produce a high coverage with pumice-like structures containing numerous internal voids (Fig. 4b).

In the PS-PED (‖) method, two different structures can be observed in the substrate. One is the pumice like structure on the top parts of the wire surface and another is the fractal structure formed in the internal sides of the wire (Fig. 5). At the top part positions of the wire in the substrate, cavitation, shock waves and microjets contributed to produce a pumice structure with large voids due to direct exposure of ultrasound effects. Herein, ultrasound plays two roles; in one hand, microstreaming and cavitation in homogenous solution (bulk, far away from the electrode surface) help to reach high weighted ions ($Bi^{+3}$) to the surface electrode and enhance the rate of deposition. In another hand, near the surface electrode (heterogeneous system), shock waves and microjets play a basic role in producing pumice like, dendrite like structures and electrode surface cleaning. While at internal spaces between the wires, cavitation and acoustic streaming led to form fractal like structures due to indirect exposure of ultrasound in the homogenous system (see Fig. 6). Elemental analysis proved the presence of Bi and S in the

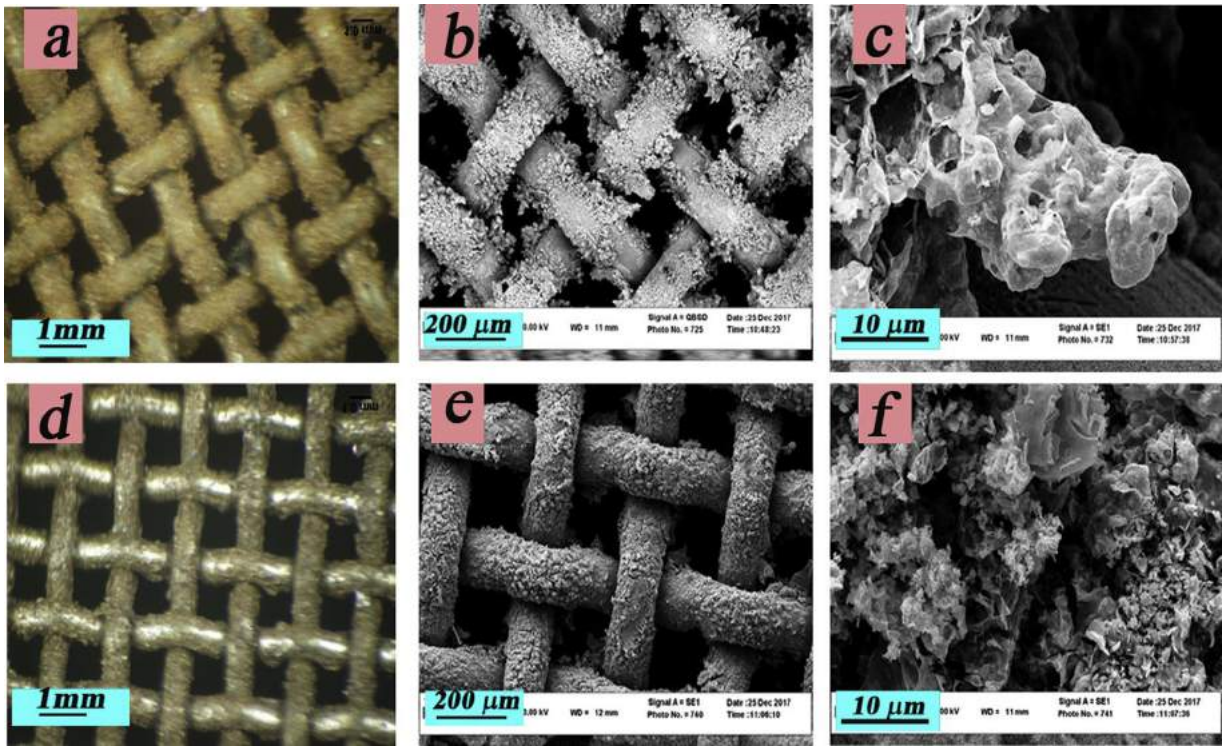


**Fig. 3.** Optical microscopy and SEM images of films obtained by PS-PED (a–c) and PED (d–f) methods.

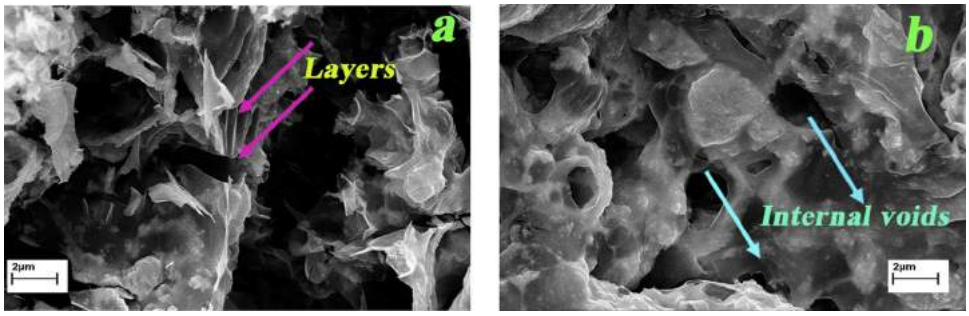


**Fig. 4.** (a) layered structure and (b) pumice like structure with internal voids films obtained by PED and PS-PED methods, respectively.

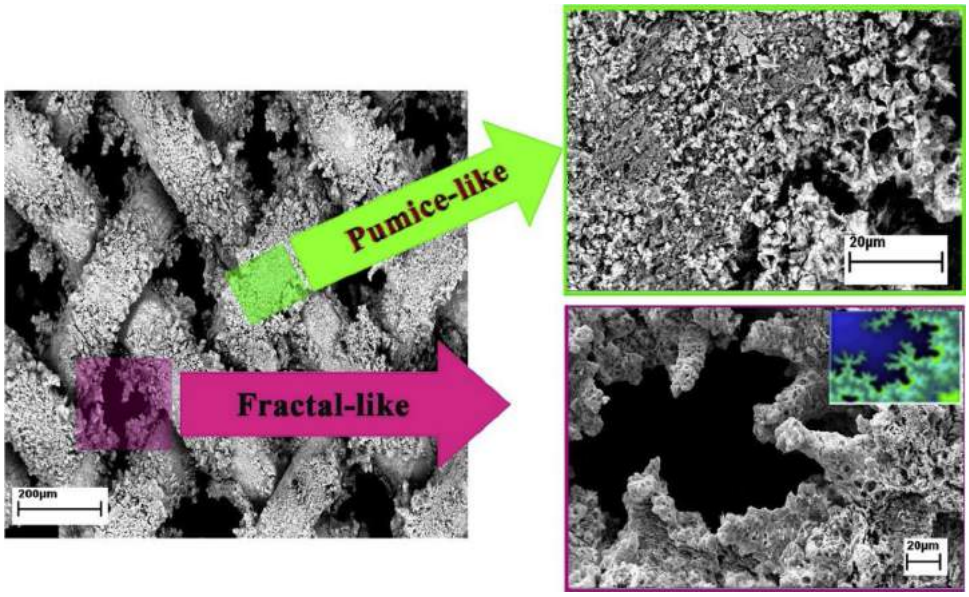


**Fig. 5.** Double structure of $Bi_2S_3$ film synthesized by PS-PED method.

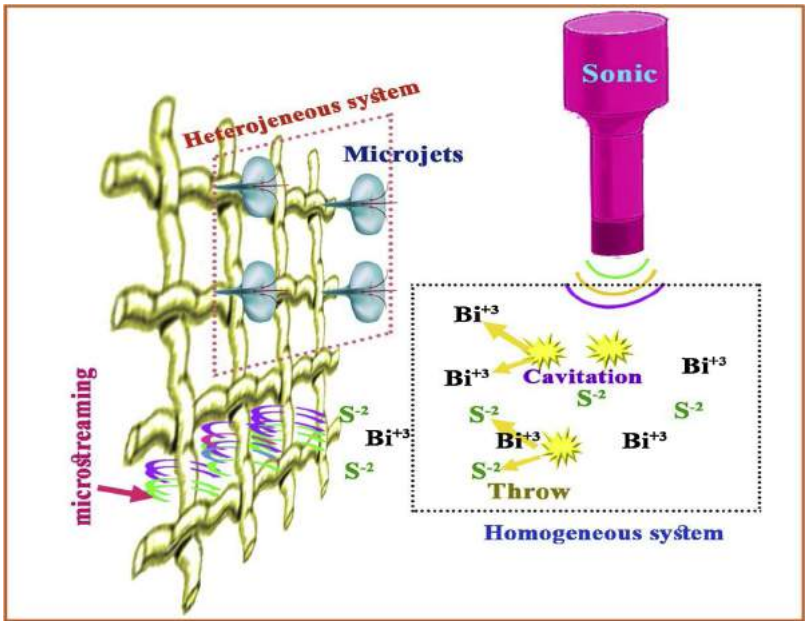


**Fig. 6.** Schematic presented the ultrasonic effects in sonodeposition process.

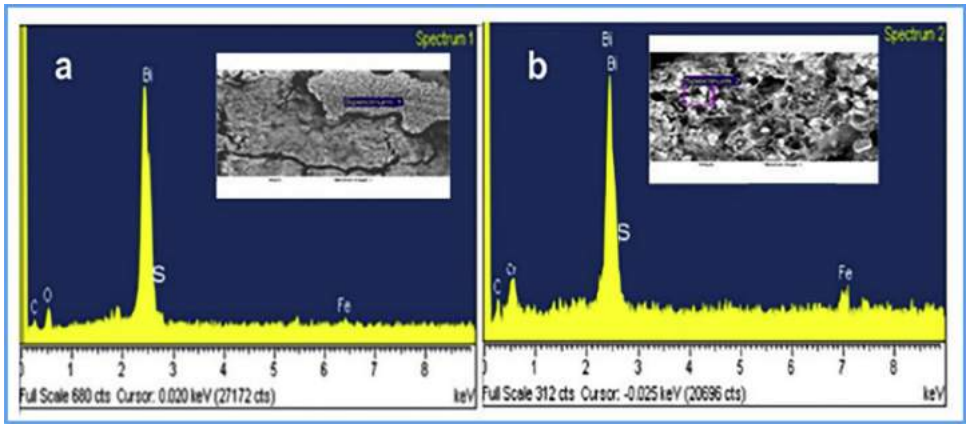


**Fig. 7.** EDS spectra for films obtained from (a) PED and (b) PS-PED methods.

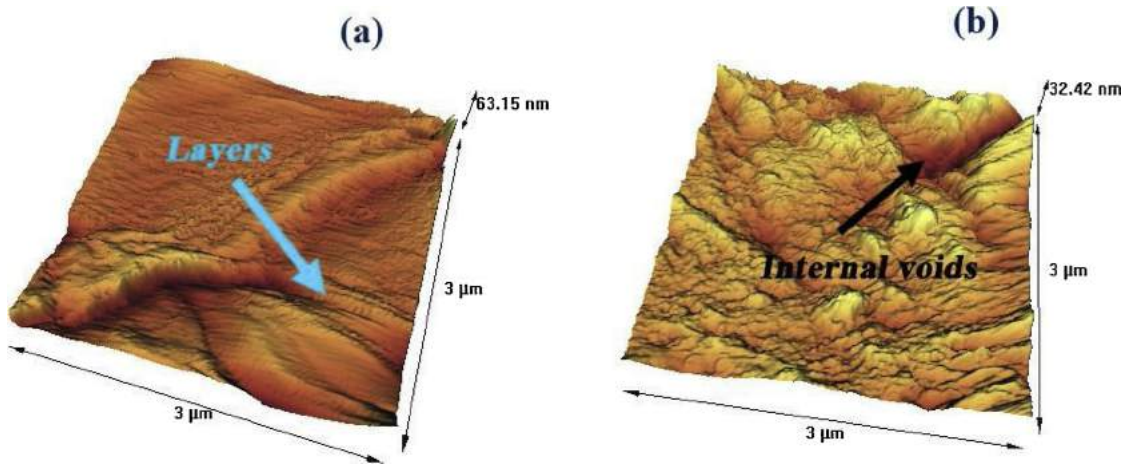


**Fig. 8.** 3D AFM images of films obtained for (a) PED and (b) PS-PED methods.

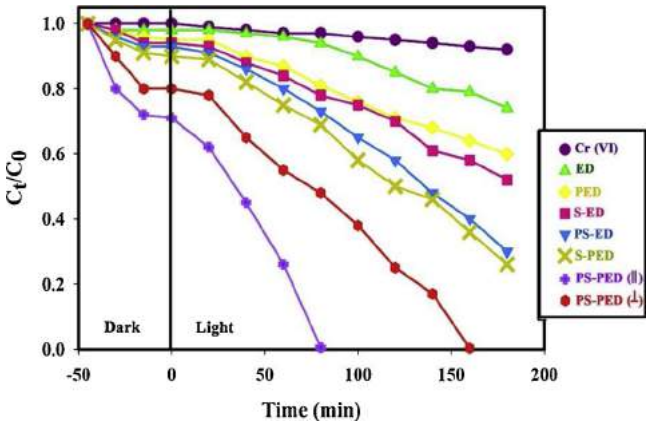


**Fig. 9.** Photocatalytic reduction of Cr (VI) by films obtained from different methods.

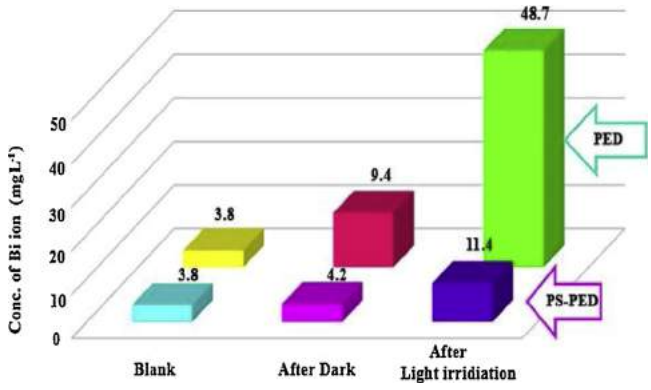


**Fig. 10.** Concentration of Bi ions measured by F-AAS for PED and PS-PED for (a) blank, (b) after dark and (c) after light irradiation.

samples by appearance the related peaks in EDS spectrum in Fig. 7(a, b). AFM images indicate that the film synthesized by the PS-PED (‖) method has a lower thickness (32.42 nm) than PED method (63.15 nm). Different thicknesses related to the use of ultrasound during the deposition that led to produce thinner films due to the cavitation process that increases the dissolution of dendrite like structures. In Fig. 8a, the film has a layer structure but Fig. 8b shows the pumice like structure with distributed internal voids.

### 3.2. Photocatalytic reduction of Cr (VI)

Fig. 9 represents the photocatalytic reduction of Cr (VI) to Cr (III) by the resultant films through various combinations of electrochemistry and ultrasound. It obviously confirmed that the film synthesized by PS-PED (‖) had the highest adsorption capacity in dark and the highest photocatalytic reduction under visible light with respect to the other films. The difference between the photocatalytic efficiencies is related to the morphology and the surface roughness of the films. To gain the optimum conditions, the best film was selected as a photocatalyst film model. The independent parameters such as $t_{on}$, $t_{off}$ and sonication

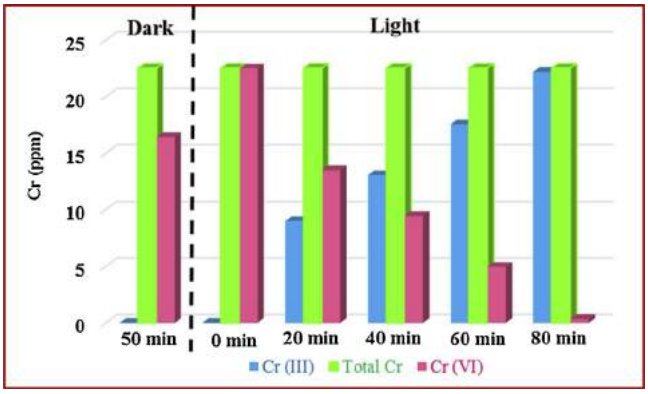


**Fig. 11.** Concertation of total Cr and Cr ions (VI, III) measured by ICP and UV–vis spectroscopies.

amplitude play essential roles on the film morphology. Therefore, the mentioned parameters were optimized by RSM. Leaching of PED and PS-PED films in the dark were studied by F-AAS by measurement of Bi ions in solution. Furthermore, photocorrosion of $Bi_2S_3$ films (PED, PS-PED) was investigated by the release of Bi ions. Concentration of Bi ions in blank solution (Cr (VI)), in dark and in photocatalytic reduction are shown in Fig. 10 for PED and PS-PED films. Blank solution (Cr (VI) without film) for both samples indicated 3.8 mg/L Bi ions. In dark, the concentration of Bi ions was 9.4 and 4.2 mg/L for PED and PS-PED, respectively. Results showed that PED sample had more leaching in solution compared to PS-PED sample. In photocatalytic process, Bi ions released in solution due to photocorrosion of $Bi_2S_3$ film for PED sample was 48.7 mg/L and for PS-PED sample was 11.2 mg/L. It could be suggested that PS-PED method for synthesis of $Bi_2S_3$ film led to reduce of its photocorrosion. To demonstrate the reduction of Cr (VI) to Cr (III), concentration of Cr ions (VI, III) and total Cr were determined for films that obtained from PS-PED (‖) method. Based on Fig. 11, it clearly indicated that total Cr through photocatalytic process was constant. After remaining for 50 min in the dark, the concentration of Cr (VI) decreased due to adsorption on the catalyst surface. Under the light, the concentration of Cr (VI) was decreased and the concentration of Cr (III) ions was increased too.

### 3.3. Fitting model

The data of photocatalytic reduction under visible light irradiation using $Bi_2S_3$ film (by PS-PED (‖)) listed in Table 3. A second-order polynomial expression consisting of 10 coefficients attained from the analysis of variance (ANOVA) at 95% confidence level ($p < 0.05$) and it shown in Eq. (3).

**Table 4**
ANOVA table obtained for photocatalytic reduction of Cr (VI).

| Source | d.f.* | Mean squares | Sum of squares | F-value | P-values |
|---|---|---|---|---|---|
| **Model** | 9 | 1531.83 | 13786.50 | 113.26 | < 0.0001 |
| **$X_1$-$t_{on}$** | 1 | 1368.90 | 1368.90 | 101.22 | < 0.0001 |
| **$X_2$-$t_{off}$** | 1 | 16.90 | 16.90 | 1.25 | 0.2898 |
| **$X_3$-S.A.**** | 1 | 22.50 | 22.50 | 1.66 | 0.2261 |
| **$X_1X_2$** | 1 | 50.00 | 50.00 | 3.70 | 0.0834 |
| **$X_1X_3$** | 1 | 200.00 | 200.00 | 14.79 | 0.0032 |
| **$X_2X_3$** | 1 | 12.50 | 12.50 | 0.92 | 0.3590 |
| **$X_1^2$** | 1 | 91.64 | 91.64 | 6.87 | 0.0264 |
| **$X_2^2$** | 1 | 346.64 | 346.64 | 25.63 | 0.0005 |
| **$X_3^2$** | 1 | 5625.14 | 5625.14 | 415.92 | < 0.0001 |
| **Residual** | 10 | 13.52 | 135.25 | | |
| **Lack of fit** | 5 | 27.05 | 135.25 | 0.46 | 0.76 |

* degree of freedom, ** sonication amplitude.

$$Y = +74.09 + 11.70X_1 - 1.30X_2 - 1.50X_3 + 2.50X_1X_2 - 5.00X_1X_3 + 1.25X_2X_3 + 5.77X_1^2 - 11.23X_2^2 - 45.23X_3^2 \quad (3)$$

where Y refers to photocatalytic reduction efficiency (%) and $X_1$, $X_2$, and $X_3$ represent the real values of $t_{on}$, $t_{off}$ and sonication amplitudes (%), respectively. Positive and negative signs before numbers in Eq. (3) indicated interactive and antagonistic effects, respectively.

The best fitting of the quadratic model in ANOVA analysis is depicted in Table 4. The large Fisher (F) value (113.26) and corresponding p-value (< 0.0001) for the estimated model indicate that the model is significant. The p-value less than 0.05 is considered to demonstrate a statistical significant model term. There is only 0.01% chance that a model F-value occurs due to noise. In addition, lack of fit (LOF) referred to data variation around the quadratic model and is always adequate proof for fitting the model (Bagheban Shahri and Niazi, 2015). Non-significant mark appeared for LOF that represents the suitability of model. The calculated F-values and p-values of each terms of model (Table 4) indicate that one independent variable ($X_1$), interactive parameter between $X_1$($t_{on}$) and $X_3$ (sonication amplitude), and three quadratic terms ($X_1^2$, $X_2^2$ and $X_3^2$) are statistically significant due to small values less than 0.05. The influence of three variables on the reduction efficiency is $X_1$ ($t_{on}$) > $X_3$ (sonication amplitude) > $X_2$ ($t_{off}$) due to F value (101.22 > 1.66 > 1.25).

Among the three variables on the photocatalytic reduction of Cr, $X_1$ ($t_{on}$) shows the highest influence due to the highest F value (101.22) and lowest p value (< 0.0001). These results are supported by the fact that the reduction efficiency would increase significantly at high level of $t_{on}$ due to deposit of large amount of photocatalyst on the substrate and increase of active sites. The negative effect of $t_{off}$ can be explained by the fact that during this period of time, dendrite like structures can be dissolved and lead to a lower thickness of the film. Furthermore, negative influence of the sonication amplitude can be attributed to the high amplitude during deposition time. This leads to dissolving and breaking of the deposited structures and causes thinning of the films. In contrast, in interactive effects, $X_1X_3$ (p-value = 0.0032) is more significant than $X_1X_2$ (p-value = 0.0834) and $X_2X_3$ (p-value = 0.3590). The negative sign of $X_1X_3$ (Eq. 3) was related to opposing effect of this interaction. Moreover, for the second-order effects, all of the three terms $X_1^2$, $X_2^2$ and $X_3^2$ are significant. Furthermore, the fit of the model is verified by the determination coefficient of $R^2$.

In this study, the value of the determination coefficient ($R^2$ = 0.9903) shown in Table 5 indicated that 99.03% of the variability in the response could be explained by the model. The adjusted determination coefficient ($R^2$ = 0.9815) is also high and indicates that the proposed model is significant. Coefficient of variance (CV) indicated reproducibility of model and value smaller than 10% is appropriate. For this model, CV value of 7.54% demonstrated low deviation between experimental and predicted values. Parameter of adequate precision (AP) calculated the signal to noise ratio, and it should be higher than 4 for the model. The calculated AP value of 33.996 shows an adequate model discrimination. Furthermore, the value of Adj-$R^2$ is close to the predicted $R^2$ value (0.9290), indicating a good relation between experimental and predicted values (reduction efficiency). Moreover, the normal probability plot of the residuals shown in Fig. 12, and it does not show any violation of the assumptions: errors are normally

**Table 5**
The values of various parameters given by RSM.

| Parameter | Std. Dev.[a] | C.V.[b]% | $R^2$ | Adj $R^2$ [c] | Pred $R^2$ [d] | Adeq Precision [e] |
|---|---|---|---|---|---|---|
| Value | 3.68 | 7.54 | 0.9903 | 0.9815 | 0.9290 | 33.996 |

[a] Standard deviation, [b] Coefficient of variation, [c] Adjusted $R^2$, [d] Predicted $R^2$, [e] Adequate precision.

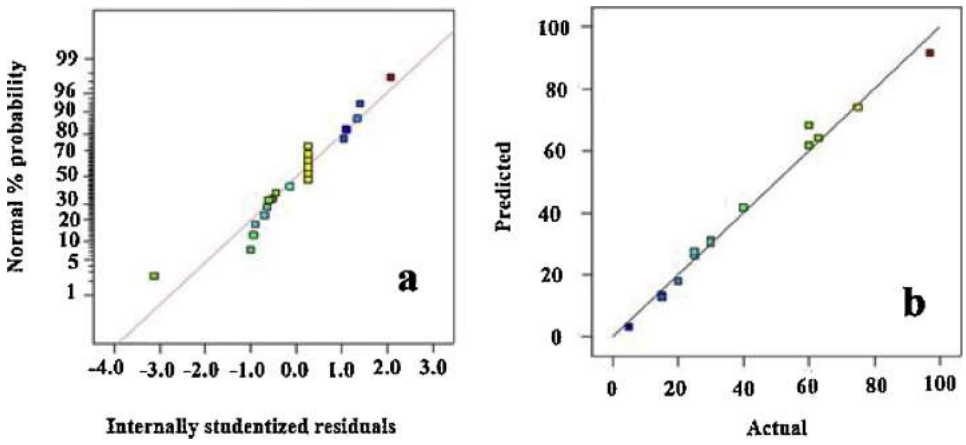


**Fig. 12.** (a) Normal probability plot of residual and (b) predicted vs. actual values plot for reduction of Cr (VI).

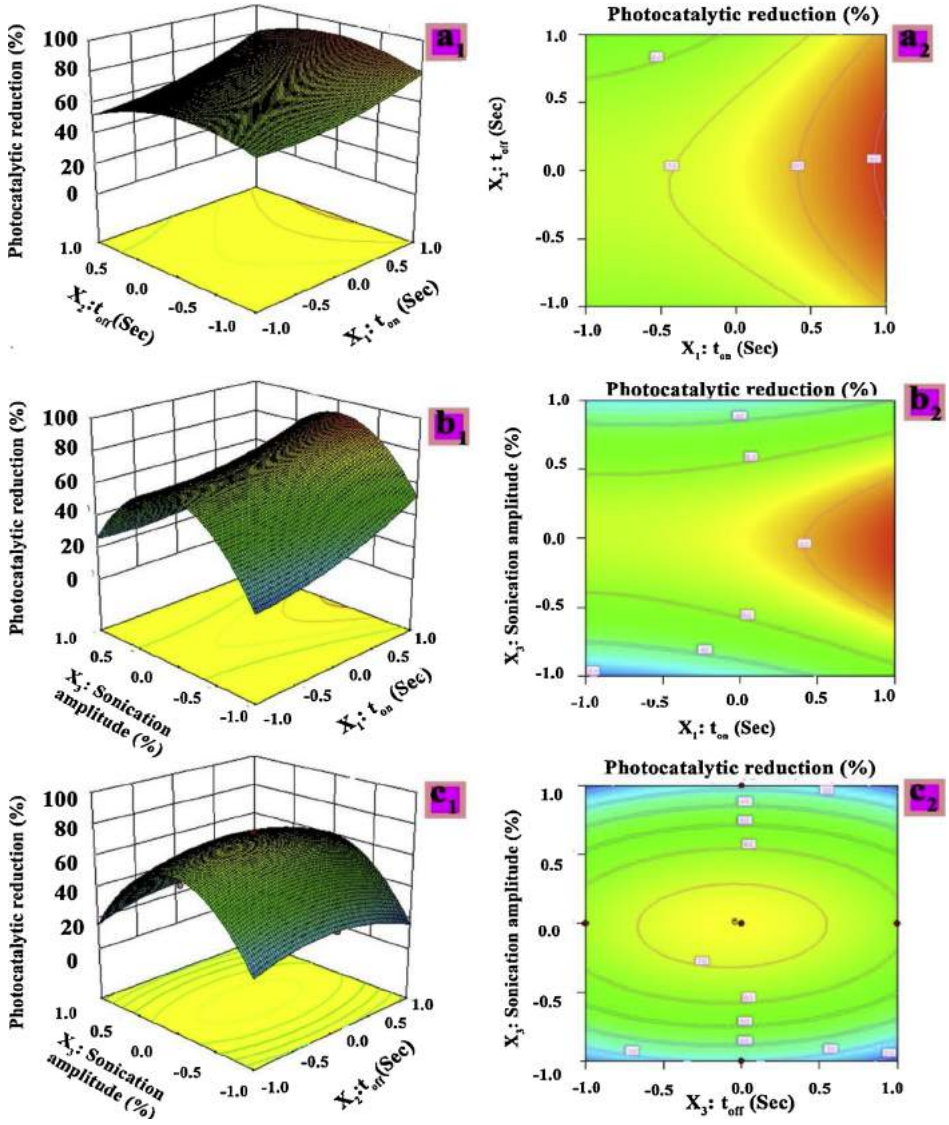


**Fig. 13.** 3D response surface and contour plots of reduction efficiency for Cr (VI) by films prepared through PS-PED method with ($a_1$) ($a_2$) $t_{on}$ and $t_{off}$, ($b_1$) ($b_2$) $t_{on}$ and sonication amplitude and ($c_1$) ($c_2$) $t_{off}$ and sonication amplitude in a fixed time (30 min).

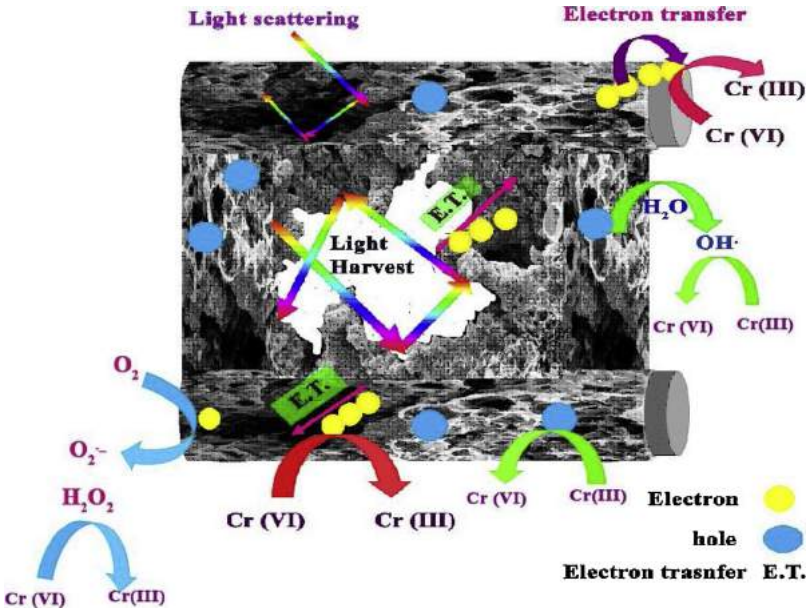


**Fig. 14.** Proposed mechanism for photocatalytic reduction of Cr (VI).

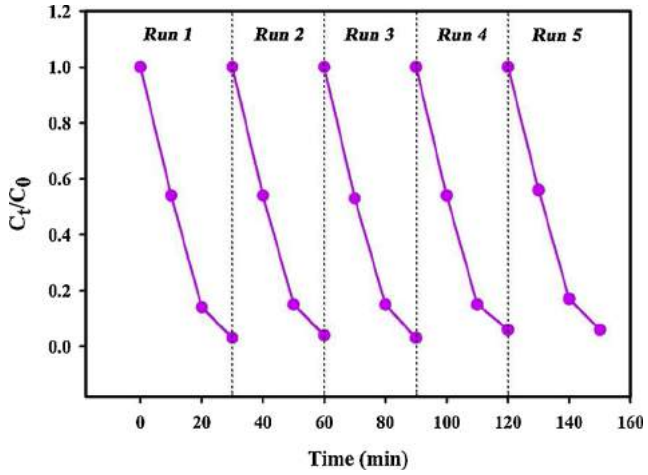


**Fig. 15.** Reusability of $Bi_2S_3$ in successive runs.

distributed and independent. Results of ANOVA could be suggesting that a quadratic polynomial model is a good model for optimization of independent parameters in preparation of films and finally in photocatalytic reduction efficiency of $Cr^{+6}$.

### 3.4. Response surface analysis

Three-dimensional (3D) and contour plots graphically shown in Fig. 13 over three independent variables ($X_1$, $X_2$ and $X_3$). The aim is to clarify the relationship between two parameters when the third parameter supposed to a fixed value at its central level. The shapes of the contour plots provide information on the nature and extent of the interactions. In a contour plot between two variables, the circular nature possibly indicates less prominent or negligible interactions while the elliptical curves are likely associated with prominent interactions. In Fig. 13, the response surface plots of photocatalytic reduction of Cr (VI) displayed for the three pairs of the factors. According to Fig. 13 ($a_1$, $a_2$), the reduction efficiency of Cr (VI) steadily improved by increasing the $t_{on}$ from 4 to 12 s. The main reason is that the deposition yield increased with higher $t_{on}$ and led to more active sites for the reduction process. Furthermore, as it concluded from these figures, Cr (VI) reduction is extremely more sensitive to changes in $t_{on}$ compared with other parameters. This is in agreement with the P-values obtained for each parameter from ANOVA table. According to Fig. 13 ($b_1$, $b_2$), the reduction efficiency of Cr (VI) improved with the increase of sonication amplitude (%) from 20 to 40% but, the efficiency was reduced from 40 to 60%. Furthermore, according to P-values obtained from ANOVA, Cr (VI) reduction is highly sensitive to changes in sonication amplitude from 20 to 60%. The main reason for this behavior is that at low sonication amplitude (20%), the nucleation rate and sending ions to double layer during deposition process are low in comparison with 40% amplitude. Compared to high sonication amplitude (> 40%), medium amplitude (40%) has high efficiency due to the main role of sonication in the porous film produced. Indeed, high amplitude caused a thinner film that is due to the corrosion of the deposited film. According to Fig. 13 ($c_1$, $c_2$), combination of $t_{off}$ and sonication amplitude had a small effect on the Cr (VI) reduction. The goal of the optimization is to minimize the final concentration of Cr (VI) in the solution. The point at which the final concentration of Cr (VI) in its lowest value is found to be at 12 s, 40%, and 8 s for $t_{on}$, sonication amplitude (%) and $t_{off}$, respectively. Based on the suggested model (Eq. (1)), the final reduction of Cr (VI) under optimal conditions should be 98.53%. To confirm the optimization studies, the experiments carried out twice again and the average final reduction efficiency in these experiments was 94.65%, which is reasonably close to the predicted value. Therefore, the optimum point determined by RSM successfully verified and suggested that RSM can be a powerful tool for optimizing photocatalytic processes.

### 3.5. Proposed mechanism and performance

According to the obtained results, the film prepared by PS-PED (‖) presented a higher efficiency compared with film prepared by PED method. Based on SEM and AFM images, the film formed by PS-PED (‖) method depicted two structures (pumice and fractal). In one hand, pumice structures composed of numerous internal voids with different sizes in its structure. Indeed, internal voids acted as sites for harvesting and multi-scattering of visible light that led to high usability of the light. This structure also provides different routes for electron transferring and separating of photogenerated hole and electrons under visible light irradiation. The effects of ultrasound such as shock waves and microjets prevented the formation of microspheres on the top of

**Table 6**
Performance of different films in photocatalytic reduction of Cr (VI).

| Film | Concentration of Cr(VI) ($mgL^{-1}$), pH | Light source | Reduction time (min) | Ref. |
|---|---|---|---|---|
| $TiO_2$ | 20, 2 | 300w, Xe lamp | 60 | (Wu et al., 2013) |
| $TiO_2$ | ...., 3 | 450w, Hg lamp | 180 | (Ananpattarachai et al., 2016) |
| $PVA/TiO_2$ | 10, ... | 300w, Xe lamp | 25 | (Yan et al., 2017) |
| $Y\text{-}TiO_2$ | 10, 2 | 30w, UV lamp | 300 | (Zhang et al., 2016) |
| $Cu_7Te_4$ | 3, 2 | 200w, W lamp | 30 | (Ghosh et al., 2016) |
| $TiO_2/ZrO_2$ | 6, 2 | Hg lamp | 30 | (Smirnova et al., 2006) |
| $Bi_2S_3$ | 45, natural | Sunlight | 30 | This work |

wires by direct sonication and produced semi-microspheres. These semi-microspheres with nanometer walls can be acted as cites for light-multiscattering and electron transferring. On the other hand, fractal like structures were able to capture the light due to sort of its structure. Indeed, these fractal structures have similarity to porous rods which have nanometer width and micrometers length due to indirect exposure of ultrasound. Fractal structures also produced routes for transferring of electrons and preventing from hole-electron recombination. Furthermore, electrons could probably transfer to the conductive substrate and prevent from recombination of charge pairs and electrons and still have enough time for reduction of Cr (VI) to Cr (III). Multiple effects of morphology and substrate have major key roles in photocatalytic reduction of Cr (VI). That is the reason that the substrate effect in the PED film compared to PS-PED exhibited lower efficiency despite the greater thickness and greater amount of catalyst. The detailed proposed mechanism is shown schematically in Fig. 14. Photogenerated holes could directly or indirectly oxidize Cr (III) to Cr (VI) by formation of hydroxyl radicals. Cr (VI) and $O_2$ molecules competed for electron capture. $O_2$ molecules take electrons and produce $O_2^{\cdot -}$ which acted as a reducing factor for reduction of Cr (VI) to Cr (III) in an indirect way. Photoelectrons can also directly reduce Cr (VI) to Cr (III).

$Bi_2S_3$ film (PS-PED (‖)) is chosen as the best sample for photocatalytic reduction of Cr (VI). Reusability of film was investigated at successive runs in photocatalytic process. After 5 cycles, the film was still showing high efficiency and stability without considerable detaching of film from the substrate (Fig. 15). The performance of $Bi_2S_3$ film in comparison with other films shown in Table 6. In this work, $Bi_2S_3$ film presents a higher efficiency than other films reported in the literature.

## 4. Conclusion

For the first time, $Bi_2S_3$ films have successfully deposited on stainless steel mesh by the sono-electrodeposition method in pulse mode. Pumice and fractal like structures have formed on the surface of substrate. These structures are favorable for photocatalytic reduction of Cr (VI) due to capability in harvesting and multi-scattering of visible light. Internal voids in pumice structure and fractals have provided routes for electron transfer. Comparison with pulse electrodeposition, ultrasound has a key role in the formation of internal voids and fractal structures. This is due to the cavitation process that produces shock waves and acoustic streaming for resolving of electrodeposition problems. Optimization of effective independent variable ($t_{on}$, $t_{off}$ and sonication amplitude) in the synthesis of films have been conducted by response surface methodology. The optimum reduction efficiency (98.53% in 30 min) was achieved by the film synthesized under conditions such as $t_{on}$ = 8 s, $t_{off}$ = 4 s and 40% sonication amplitude.

## Acknowledgement

The support of Ferdowsi University of Mashhad (Research and Technology), Iran for this work (3/39052) is appreciated.

## References

Ananpattarachai, J., Paksaharn, P., Kajitvichyanukul, P., 2016. Photocatalytic reduction of chromium (VI) in aqueous solutions by nano-TiO2 thin film in rotating disc photoreactor. Int. J. Environ. Waste Manag. 17, 176. https://doi.org/10.1504/IJEWM.2016.076754.

Bagheban Shahri, F., Niazi, A., 2015. Synthesis of modified maghemite nanoparticles and its application for removal of Acridine Orange from aqueous solutions by using Box-Behnken design. J. Magn. Magn. Mater. 396, 318–326. https://doi.org/10.1016/j.jmmm.2015.08.054.

Buzea, C., Pacheco, I.I., Robbie, K., 2007. Nanomaterials and nanoparticles: Sources and toxicity. Biointerphases 2, MR17–MR71. https://doi.org/10.1116/1.2815690.

Chandrasekar, M.S., Pushpavanam, M., 2008. Pulse and pulse reverse plating-Conceptual, advantages and applications. Electrochim. Acta 53, 3313–3322. https://doi.org/10.1016/j.electacta.2007.11.054.

Ganesan, R., Shanmugam, S., Gedanken, A., 2008. Pulsed sonoelectrochemical synthesis of polyaniline nanoparticles and their capacitance properties. Synth. Met. 158, 848–853. https://doi.org/10.1016/j.synthmet.2008.06.001.

Gao, C., Shen, H., Sun, L., Shen, Z., 2011. Chemical bath deposition of Bi2S3films by a novel deposition system. Appl. Surf. Sci. 257, 7529–7533. https://doi.org/10.1016/j.apsusc.2011.03.080.

Georges, C., Tena-Zaera, R., Bastide, S., Rouchaud, J.C., Larramona, G., Lévy-Clément, C., 2007. Electrochemical deposition of Bi[sub 2]S[sub 3] thin films using dimethylsulfoxide as a solvent. J. Electrochem. Soc. 154, D669. https://doi.org/10.1149/1.2792244.

Ghosh, A., Mitra, M., Banerjee, D., Mondal, A., 2016. Facile electrochemical deposition of Cu7Te4thin films with visible-light driven photocatalytic activity and thermoelectric performance. RSC Adv. 6, 22803–22811. https://doi.org/10.1039/c6ra00345a.

González-García, J., Esclapez, M.D., Bonete, P., Hernández, Y.V., Garretón, L.G., Sáez, V., 2010. Current topics on sonoelectrochemistry. Ultrasonics. 50, 318–322. https://doi.org/10.1016/j.ultras.2009.09.022.

Holmes, A.L., Wise, S.S., Wise Sr., J.P., 2008. Carcinogenicity of hexavalent chromium. Indian J. Med. Res. 128, 353–372.

Hansen, M.B., Johansen, J.D., Menne, T., 2003. Chromium allergy : significance of both Cr (III) and Cr (VI). Contact Derm. 49, 206–212.

Jana, A., Bhattacharya, C., Sinha, S., Datta, J., 2009. Study of the optimal condition for electroplating of Bi 2S 3 thin films and their photoelectrochemical characteristics. J. Solid State Electrochem. 13, 1339–1350. https://doi.org/10.1007/s10008-008-0679-z.

Jin, J., He, T., 2017. Facile synthesis of Bi2S3nanoribbons for photocatalytic reduction of CO2into CH3OH. Appl. Surf. Sci. 394, 364–370. https://doi.org/10.1016/j.apsusc.2016.10.118.

Kloke, A., Von Stetten, F., Zengerle, R., Kerzenmacher, S., 2011. Strategies for the fabrication of porous platinum electrodes. Adv. Mater. 23, 4976–5008. https://doi.org/10.1002/adma.201102182.

Li, D.B., Hu, L., Xie, Y., Niu, G., Liu, T., Zhou, Y., Gao, L., Yang, B., Tang, J., 2016. Low-temperature-processed amorphous Bi2S3 Film as an inorganic Electron transport layer for perovskite solar cells. ACS Photonics 3, 2122–2128. https://doi.org/10.1021/acsphotonics.6b00582.

Li, H., Gong, Y., Huang, Q., Zhang, H., 2013. Degradation of orange II by UV-assisted advanced fenton process: response surface approach, degradation pathway, and biodegradability. Ind. Eng. Chem. Res. 52, 15560–15567. https://doi.org/10.1021/ie401503u.

Luo, S., Qin, F., Ming, Y., Zhao, H., Liu, Y., Chen, R., 2017. Fabrication uniform hollow Bi2S3nanospheres via Kirkendall effect for photocatalytic reduction of Cr(VI) in electroplating industry wastewater. J. Hazard. Mater. 340, 253–262. https://doi.org/10.1016/j.jhazmat.2017.06.044.

Nasiri Vatan, H., Mohammad Shafiee, M., Khanfekr, A., Laleh, M., Kaffashan, H., Jafarzadeh, K., 2014. Optimisation of experimental conditions for pulse electrodeposition of nanostructured platinum. Surf. Eng. 30, 89–96. https://doi.org/10.1179/1743294413Y.0000000228.

Otsuka, E., Kurumada, K., Suzuki, A., Matsuzawa, S., Takeuchi, K., 2008. An application of transparent mesoporous bulk silica to a titanium dioxide photocatalyst with adsorption and decomposition functions. J. Solgel Sci. Technol. 46, 71–78. https://doi.org/10.1007/s10971-008-1688-1.

Sáez, V., Mason, T.J., 2009. Sonoelectrochemical synthesis of nanoparticles. Molecules 14, 4284–4299. https://doi.org/10.3390/molecules14104284.

Shen, Q., Jiang, L., Miao, J., Hou, W., Zhu, J.J., 2008. Sonoelectrochemical synthesis of

CdSe nanotubes. Chem. Commun. 1683–1685. https://doi.org/10.1039/b718022e.
Smirnova, N., Gnatyuk, Y., Eremenko, A., Kolbasov, G., Vorobetz, V., Kolbasova, I., Linyucheva, O., 2006. Photoelectrochemical characterization and photocatalytic properties of mesoporous TiO2/ZrO2films. Int. J. Photoenergy 2006, 1–6. https://doi.org/10.1155/IJP/2006/85469.
Song, Y.J., Oh, J.K., Park, K.W., 2008. Pt nanostructure electrodes pulse electrodeposited in PVP for electrochemical power sources. Nanotechnology 19, 355602–355608. https://doi.org/10.1088/0957-4484/19/35/355602.
Taguchi, M., Schwalb, N., Rong, Y., Vanegas, D.C., Garland, N., Tan, M., Yamaguchi, H., Claussen, J.C., McLamore, E.S., 2016. PulSED: Pulsed sonoelectrodeposition of fractal nanoplatinum for enhancing amperometric biosensor performance. Analyst 141, 3367–3378. https://doi.org/10.1039/c6an00069j.
Velanganni, S., Manikandan, A., Prince, J.J., Mohan, C.N., Thiruneelakandan, R., 2018. Nanostructured ZnO coated Bi2S3thin films: enhanced photocatalytic degradation of methylene blue dye. Phys. B Condens. Matter. 545, 383–389. https://doi.org/10.1016/j.physb.2018.07.005.
Wu, Q., Zhao, J., Qin, G., Wang, C., Tong, X., Xue, S., 2013. Photocatalytic reduction of Cr (VI) with TiO2film under visible light. Appl. Catal. B Environ. 142–143, 142–148. https://doi.org/10.1016/j.apcatb.2013.04.056.
Xu, S., Dai, J., Yang, J., You, J., Hao, J., 2018. Facile synthesis of novel CaIn2S4/ZnIn2S4 composites with efficient performance for photocatalytic reduction of Cr(VI) under simulated sunlight irradiation. Nanomaterials 8, 472. https://doi.org/10.3390/nano8070472.
Yan, W., Chen, Q., Meng, X., Wang, B., 2017. Multicycle photocatalytic reduction of Cr (VI) over transparent PVA/TiO2nanocomposite films under visible light. Sci. China Mater. 60, 449–460. https://doi.org/10.1007/s40843-017-9024-9.
Zargazi, M., Entezari, M.H., 2018. BFO thin film on the stainless steel mesh by anodic EPD: a visible light photocatalyst for degradation of Rhodamin B. J. Photochem. Photobiol. A: Chem. 365, 185–198. https://doi.org/10.1016/j.jphotochem.2018.07.042.
Zargazi, M., Entezari, M.H., 2019a. Sonochemical versus hydrothermal synthesis of bismuth tungstate nanostructures: photocatalytic, sonocatalytic and sonophotocatalytic activities. Ultrason. Sonochem. 51, 1–11. https://doi.org/10.1016/j.ultsonch.2018.10.010.
Zargazi, M., Entezari, M.H., 2019b. Anodic electrophoretic deposition of $Bi_2WO_6$ thin film : high photocatalytic activity for degradation of a binary mixture. Appl. Catal. B Environ. 242, 507–517. https://doi.org/10.1016/j.apcatb.2018.09.093.
Zhang, Q., Fu, Y., Wu, Y., Zhang, Y.N., Zuo, T., 2016. Low-cost Y-Doped TiO2Nanosheets film with highly reactive {001} facets from CRT waste and enhanced photocatalytic removal of Cr(VI) and methyl orange. ACS Sustain. Chem. Eng. 4, 1794–1803. https://doi.org/10.1021/acssuschemeng.5b01783.